Inertioelastic Poiseuille flow over a wavy surface

Rapid Communications

Inertioelastic Poiseuille flow over a wavy surface

Simon J. Haward,[1] Jacob Page,[2,3] Tamer A. Zaki,[4] and Amy Q. Shen[1]
[1]*Okinawa Institute of Science and Technology Graduate University, 1919-1 Tancha, Onna-son, Okinawa 904-0495, Japan*
[2]*School of Mathematics, University of Bristol, Bristol BS8 1TW, United Kingdom*
[3]*Department of Applied Mathematics and Theoretical Physics, University of Cambridge, Centre for Mathematical Sciences, Wilberforce Road, Cambridge CB3 0WA, United Kingdom*
[4]*Department of Mechanical Engineering, Johns Hopkins University, Baltimore, Maryland 21218, USA*

(Received 22 January 2018; revised manuscript received 29 March 2018; published 21 September 2018)

Streamwise boundary undulations induce spanwise vorticity in flows. In Newtonian flow, vorticity decays exponentially with distance from the undulation. However, recent theory for inertioelastic polymeric flow predicts vorticity amplification in a "critical layer" far from the site of disturbance. Here we present the first experimental evidence for the existence of such critical layers, demonstrating their measurable role in real polymeric flows with inertia. These vorticity amplification effects should be considered in all evaluations of vorticity dynamics in inertioelastic flows with streamline curvature.

DOI: 10.1103/PhysRevFluids.3.091302

The addition of even minute quantities (parts per million, ppm) of high-molecular-weight flexible polymers to a Newtonian solvent imparts a small but important degree of elasticity to the fluid, dramatically modifying its macroscopic flow behavior. Some well-known examples are the increase of the pressure drop measured across porous beds [1,2], the reduction of turbulent drag [3–5], and the modification of jet breakup, spray atomization, and drop impact behavior [6–8].

In the context of turbulent drag reduction, dilute polymer additives dampen streamwise vorticity via a mechanism attributed to a resistive polymer torque (the curl of the polymer force) [9–11]. However, recent experiments and simulations indicate that such fluids can support an entirely new elastoinertial turbulence (EIT) dominated by spanwise vorticity rolls [12,13]. While EIT is thought to share mechanistic similarities with purely elastic instabilities and elastic turbulence [14,15], EIT clearly depends on inertia, and the details of the interactions underpinning the resulting self-sustaining chaotic motion remain to be fully explained.

The influence of fluid elasticity on spanwise vorticity is less well understood than its effect on streamwise rolls. However, the dominance of spanwise-coherent structures in EIT suggests their important role in drag reduction. Spanwise vorticity can be generated by streamwise undulations in flow, which can be introduced in a controlled way by employing a regular wavy surface. Recent linear theory for polymer solutions in simple shear demonstrates that even small-amplitude waviness can cause significant vorticity amplification in critical layers located some distance away from the wavy surface where vorticity is injected [16]. This is fundamentally different

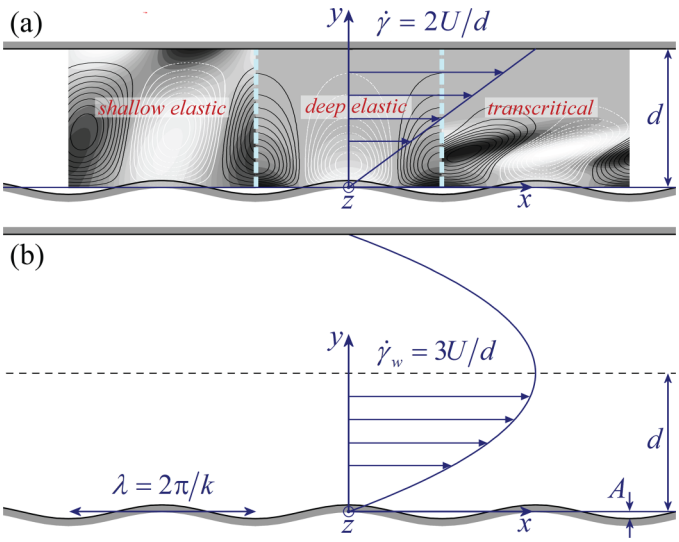

FIG. 1. (a) Schematic representation of Couette flow over a wavy surface, indicating the nature of vorticity perturbations predicted in the three regimes of viscoelastic flow [16]. (b) Schematic representation of Poiseuille flow over a wavy surface, as employed in the present study.

from Newtonian behavior and contrasts with the suppression of streamwise vorticity commonly attributed to polymer additives.

In this Rapid Communication, we provide the first experimental evidence supporting the theoretical prediction of such critical layers in inertial flows of dilute polymer solutions over undulating surfaces. The confirmation that these critical layers exist and are observable in real polymeric flows has important implications for understanding the dynamics of other inertioelastic flows, since it suggests that both the propagation of spanwise vorticity disturbances along mean-flow streamlines carrying elastic tensile stress and the associated mechanism for vorticity amplification are important physical effects that have been overlooked.

Linear perturbation theory has shown that for Newtonian flow in a plane-Couette geometry of gap depth d, the spanwise vorticity induced by a sinusoidal perturbation to the wall profile (wavelength λ, wave number $k = 2\pi/\lambda$, amplitude $A \ll d$ and $A \ll \lambda$, Fig. 1) is maximal at the surface and decays monotonically within a distance $\approx 1/k$ from the wavy wall [16,17]. However, applying linear perturbation to the Oldroyd-B viscoelastic constitutive model in the same wavy plane-Couette, Page and Zaki predicted the existence of a critical layer at some finite distance $l_c = \sqrt{2\eta_p \tau/\rho}$ from the wall, where ρ is the density, η_p is the polymeric contribution to the total viscosity, and τ is the relaxation time of the fluid [16]. Within the critical layer, amplification of the vorticity occurs. Theory indicates that the vorticity amplification is driven by a kinematic mechanism attributed to the polymer torque [16].

The emergence of viscoelastic critical layers was also examined in earlier work by Joseph and coworkers [18–21]. For example, Hu and Joseph [21] (and also Delvaux and Crochet [22]) performed numerical simulations of the flow of an upper-convected Maxwell (UCM) fluid past a cylindrical obstacle and observed that the drag plateaus above a critical flow rate, while Yoo and Joseph [19] examined a viscoelastic channel flow with wavy surfaces, a configuration similar to that considered in the present study. In both cases, an observed modulation of the vorticity field was attributed to a change in type of the governing equations from elliptic to hyperbolic in the flow domain across a critical layer where the flow velocity exceeds an elastic shear wave speed, $c_s = \sqrt{\eta_p/\tau}$. In contrast, the critical layer predicted by Page and Zaki [16] is the surface at which the base-flow velocity is equal to the elastic vorticity wave speed, $c_\omega = \sqrt{\eta_p T_{11}/\rho}$, where T_{11} is the

base-state streamwise-normal polymer stress. This wave speed is associated with the propagation of vorticity fluctuations along the tensioned mean-flow streamlines.

In the framework described by Page and Zaki [16], the flow domain and critical layer depths can be normalized by the wave number k to provide a pair of dimensionless parameters, $\alpha = kd$ and $\Sigma = kl_c$, spanning a phase diagram that can be divided into three broad regimes. In the Couette geometry, a shallow elastic regime [see Fig. 1(a)] is defined by the conditions $\alpha \lesssim 1$ and $\Sigma \gtrsim \alpha$: Here the perturbations induced by the wavy surface fill the flow domain, but the critical layer is outside of the domain ($l_c > d$) and does not influence the flow field. A deep elastic regime [Fig. 1(a)] occupies the region of the phase diagram defined by $\alpha \gtrsim 1$ and $\Sigma \gtrsim 1$: In this regime, perturbations decay within the flow domain, but the critical layer exists outside the region occupied by the perturbation and thus the flow field again appears pseudo-Newtonian.

Note that in a Newtonian flow, three regimes of penetration also exist in all of which the vorticity maximum is located at the wall [17]. The controlling parameters are α and $\theta = (\eta_s k^2/\beta\rho\dot{\gamma})^{1/3} = (2\alpha^2/3\,\mathrm{Re})^{1/3}$. Here, the Reynolds number is defined as $\mathrm{Re} = 2\rho U d\beta/\eta_s$, where $\beta = \eta_s/\eta_0$ is the solvent-to-total-viscosity ratio with the zero shear viscosity $\eta_0 = \eta_s + \eta_p$ (η_s is the solvent contribution), and $\dot{\gamma}$ is the shear rate [see Fig. 1(a)]. Physically, θ is a normalized viscous length scale that characterizes the thickness of the vortical region. In the non-Newtonian flows, Σ replaces θ as the controlling parameter in the phase diagram. The transition to this viscoelastic framework is not universal for all viscoelastic flows. Crucially, the viscoelastic picture requires that the Weissenberg number, $\mathrm{Wi} = \dot{\gamma}\tau$, is sufficiently large so that the streamwise-normal polymer stress dominates and relaxation can be neglected. In this case, θ is of secondary importance. However, if Wi is small, the rapid relaxation of the polymer means that quasi-Newtonian behavior is observed, with θ still important at leading order. In the present configuration, both Wi and Re grow linearly with the flow rate, while Σ is fixed for a given set of fluid properties. Therefore, for a given channel configuration, α, there will be a flow rate associated with a "critical" value of Wi (and Re) above which the α-Σ viscoelastic phase diagram emerges. As such, the viscoelastic framework is anticipated to appear below a threshold $\theta = \theta_c$.

The normalized critical layer depth, Σ, is related to the elasticity number $\mathrm{El} = (1-\beta)\mathrm{Wi}/\mathrm{Re}$ via $\Sigma = kd\sqrt{2\mathrm{El}}$. Interestingly, the deep and shallow elastic regimes arise for relatively high values of El (typical of more concentrated polymer solutions), which would intuitively, and in this case erroneously, be expected to exhibit strong non-Newtonian behavior. For more weakly elastic fluids with low values of El such that $\Sigma \lesssim \alpha$ (i.e., $l_c < d$) and $\Sigma \lesssim 1$, the critical layer is located both within the flow domain *and* within the distance of order $1/k$ from the wavy wall over which the perturbations decay. In this "transcritical" regime, the extra vorticity generated within the critical layer is manifested, see Fig. 1(a); hence, if the theory is correct, its influence on the flow field should in principle be observable experimentally.

Because of experimental difficulties in employing the plane-Couette configuration, here we use microfabricated rectangular glass channels which have one wavy wall, and hence the base flow state is Poiseuille. Figure 1(b) provides a schematic representation of the problem setup. A minor, but notable, difference from the Couette configuration is that here we consider the depth of the flow domain d to be one-half of the total channel depth, and hence there is no solid no-slip boundary at the location $y = d$ [23]. Experiments with Newtonian fluids have shown that in this case deep channels are those with $\alpha \gtrsim \pi$ and shallow channels are those with $\alpha \lesssim \pi$. Further, since the shear rate in Poiseuille flow varies across the flow domain, we consider the nominal wall value $\dot{\gamma}_w = 3U/d$ as representative. Two distinct channels are employed in the flow experiments: both have a depth of $d = 0.2$ mm through y and spanwise width of $w = 2$ mm through z. These dimensions provide a high aspect ratio of $r_a = w/2d = 5$ and hence a good approximation to a two-dimensional (2D) planar flow profile near the channel midwidth ($z = w/2$). The channels each have one sinusoidal wavy surface located at the mean-position $y = 0$ plane and with amplitude $A = 0.01$ mm. However, the two channels have distinct wavelengths on the wavy wall: one of the channels is deep with $\lambda = 0.125$ mm ($\alpha = 3.2\pi \approx 10$), and the other is shallow with $\lambda = 1.25$ mm ($\alpha = 0.32\pi \approx 1$). The fabrication of the glass channels by selective laser-induced etching [24] has been described

TABLE I. Salient parameters of the polymeric test fluids.

Fluid	η_0 [mPa s]	β	τ [ms]	$\Sigma_{\alpha\sim1}$	$\Sigma_{\alpha\sim10}$
A	0.91	0.96	5	0.1	1.0
B	9.48	0.81	145	3.6	36

in more details in our previous publication [23]. The same channels have been tested for flows of Newtonian fluids over a wide range of Reynolds numbers and the results compared favorably with the predictions of linear perturbation theory [16,23].

Two polymer solutions are employed in the flow experiments, both prepared using poly(ethylene oxide) (PEO, molecular weight $M = 4$ MDa, Sigma-Aldrich). Fluid A is composed of 30 ppm PEO dissolved in deionized (DI) water and is considered weakly elastic with El ≈ 0.007. Fluid B is of higher El ≈ 9.4 and is composed of 300 ppm PEO dissolved in a more viscous Newtonian solvent formed from DI water with 13 000 ppm poly(ethylene glycol) (PEG, $M = 8$ kDa, Sigma-Aldrich). The two Newtonian solvents have viscosities and densities of $\eta_s = 0.87$ mPa s, $\rho = 996.9$ kg m^{-3} (DI water) and $\eta_s = 7.72$ mPa s, $\rho = 1015.5$ kg m^{-3} (13 000 ppm PEG in DI water) and are the same as those examined in our previous work [23]. The viscosities of the polymer solutions have been measured at 25°C in a cone-and-plate rotational rheometer (DHR3, TA Instruments Inc.) and do not vary over approximately two decades of shear rate. The relaxation times of the polymer solutions have been measured by capillary breakup measurements performed on a CaBER 1 extensional rheometer (Thermo-Haake). The densities of the polymer solutions are assumed to be the same as the respective solvent. Relevant parameters for both polymeric test fluids and the resulting values of the dimensionless critical layer depth in each of the two flow channels are provided in Table I. While transcritical behavior requires both strong inertial and elastic forces (as described by Re and Wi, respectively), it can be shown that, for this Poiseuille flow, $\Sigma/\alpha = \sqrt{4\mathrm{El}/3} \lesssim 1$, and hence that El $\leqslant 0.75$ in order to observe transcritical phenomena (for $\Sigma = \alpha \leqslant \pi$). Clearly, the parameters of fluid A satisfy these conditions [16]. Fluid B, on the other hand, has $\Sigma > \alpha$, and hence shallow elastic and deep elastic behavior might be expected in the channel with $\alpha < \pi$ and $\alpha > \pi$, respectively. It is apparent from Table I that for fluid A the critical layer location is $\Sigma = 0.1\alpha$ (or $l_c = 0.1d$) from the wavy wall. Assuming a 2D parabolic velocity profile through the channel depth, the shear rate at this location is $0.9\dot{\gamma}_w$. The small variation in shear rate between $y = 0$ and $y = l_c$ indicates that the choice of $\dot{\gamma}_w$ as a characteristic value is reasonable in this case.

Flow through the devices is driven along the x direction at controlled average flow velocity U using a high-precision neMESYS syringe pump (Cetoni GmbH). Spatially resolved microparticle image velocimetry (μ-PIV, TSI Inc) is used to measure velocity vector fields at the midwidth ($z = w/2$) of the wavy channels as the flow rate is varied for both the polymer solutions and the solvents, providing velocity vector components u and v in the x and y directions, respectively [23,25,26]. Since for a Poiseuille flow over a smooth surface, $v_{Pois} \equiv 0$, perturbations to v induced by the wavy surface are readily apparent and thus $v' = v - v_{Pois} \equiv v$. Various efforts were made to evaluate the u' perturbation component by subtraction of assumed base flow profiles from the velocimetry data, and hence to obtain the full vorticity perturbation $\omega' = \partial v'/\partial x - \partial u'/\partial y$. However, such approximations are found to fail either in the vicinity of the wall or at higher Re, which are the locations and regimes of chief importance as Σ and θ become small. Furthermore, pointwise numerical differentiation of the small perturbation velocity components required to compute ω' severely degrades the signal-to-noise ratio. Hence, as in previous work with Newtonian fluids [23], we characterize perturbations to the flow field experimentally using only the v' component, which is extracted directly from the velocimetry with great reliability and confidence.

Figure 2 shows the results of μ-PIV measurements made at various values of θ in the deep wavy channel ($\alpha = 3.2\pi$). For Newtonian fluid [Fig. 2(a)] at high $\theta \gtrsim 1$ (low Re), the v' perturbation

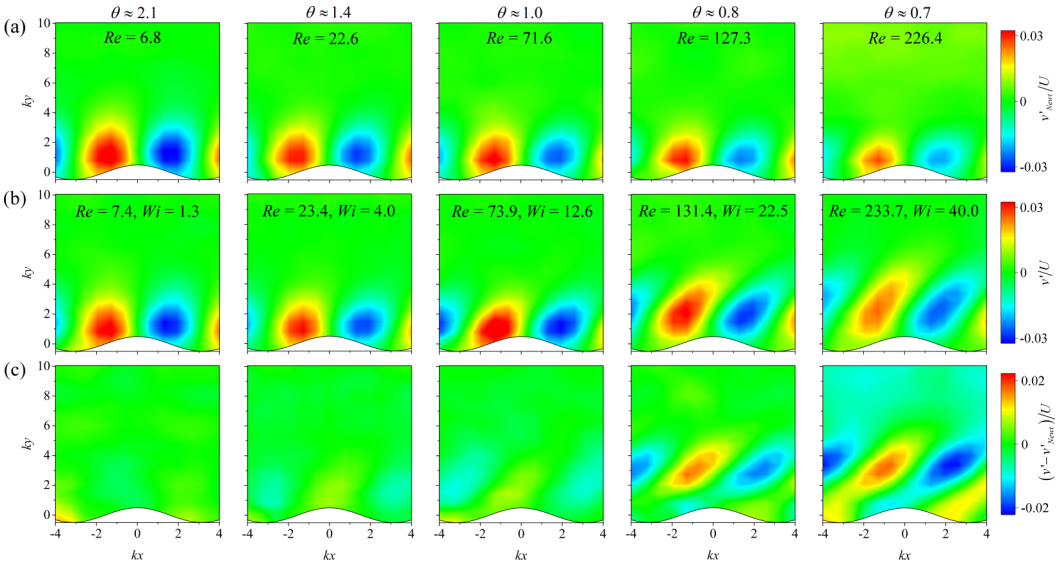

FIG. 2. Normalized y-velocity component perturbations v'/U in the wavy walled channel with $\alpha = 3.2\pi$ at the dimensionless viscous length scale θ indicated at the top. (a) Newtonian fluid ($\Sigma = 0$) at the indicated Re. (b) Polymeric fluid A ($\Sigma = 1.0$) at the indicated Re and Wi. (c) Difference between the polymeric and the Newtonian response at each θ value.

is consistent with deep viscous behavior reported previously [16,17,23]. As Re is increased and θ decreases below ≈ 1, the fluid displays inviscid behavior and the perturbation is increasingly localized toward the wavy surface and decreases in magnitude [23]. For polymeric fluid A [$\Sigma = 1.0$, Fig. 2(b)], quite different behavior is observed as θ is progressively decreased. Here, for $\theta \gtrsim 1$ (i.e., low Re and low Wi) the perturbations appear Newtonian-like; however, for $\theta \lesssim 1$ the perturbation is distorted in shape in a distinctly different manner from the Newtonian case and penetrates more deeply into the channel. Differences between the observed Newtonian and polymeric responses are rendered more apparent by performing a subtraction, as shown in Fig. 2(c). At high θ, there is negligible difference between the two fluids, confirming the pseudo-Newtonian response of the polymer solution. However, for lower values of θ, Fig. 2(c) shows that the polymeric response is composed of a Newtonian part and a significant extra, non-Newtonian, contribution with a maximum located some distance from the wavy wall.

The v' perturbation component is used to evaluate an experimental measure of the penetration depth $\mathcal{P}$ of the disturbance [16,23]:

$$\mathcal{P} \equiv ky(\Lambda = 0.95), \text{ where } \Lambda(y) = \frac{\int_0^y |v'(s)|^2 ds}{\int_0^d |v'(s)|^2 ds}. \tag{1}$$

Figure 3 shows the results of the experimental penetration depth measurements made for all the various test fluids in both of the wavy channels over a range of θ. The penetration depth of perturbations in Newtonian fluid ($\Sigma = 0$) in the deep ($\alpha = 3.2\pi$) and shallow ($\alpha = 0.32\pi$) channels is indicated by the solid black and gray lines, respectively. For the most elastic polymer solution, fluid B, in the shallow channel ($\Sigma = 3.6$), the penetration depth appears Newtonian-like, which is consistent with the prediction of shallow elastic behavior with $\alpha \lesssim \pi$, $\Sigma \gtrsim \alpha$.

In the deep channel, the penetration of fluid B ($\Sigma = 36$) is again essentially Newtonian-like in the high-θ plateau region, which is as predicted for deep elastic type behavior with $\alpha \gtrsim \pi$, $\Sigma \gtrsim \pi$ [16].

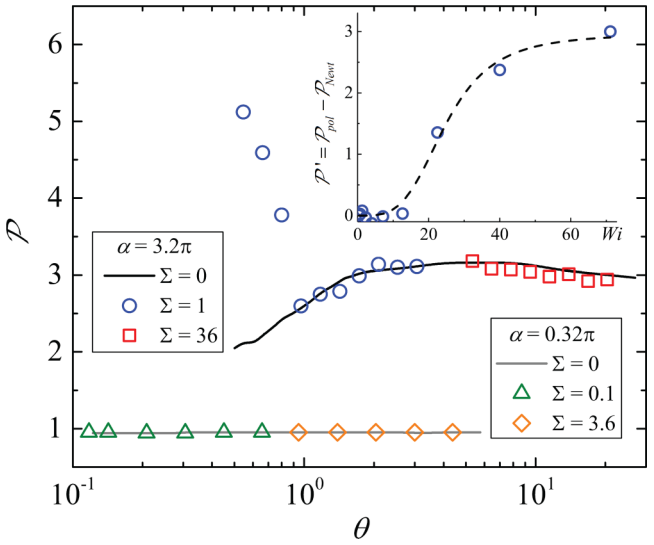

FIG. 3. Penetration depth $\mathcal{P}$ as a function of the viscous length θ for Newtonian and polymeric fluids in the deep and shallow channels. Inset shows the difference between the penetration of fluid A and that of the Newtonian fluid in the deep channel as a function of the Weissenberg number for the polymeric flow. The sigmoidal dashed line is to guide the eye.

However, fluid A in the deep channel has parameters ($\alpha = 3.2\pi$, $\Sigma = 1.0$) which correspond to the requirements for observation of *transcritical* behavior. The analysis in [16] indicates that the vorticity amplification associated with this regime only occurs when θ is small (solvent diffusion cannot smooth the critical layer) and Wi is large (strong tension in the streamlines) with $\Sigma \sim 1$. These predictions are consistent with the results reported in Fig. 3: The Newtonian-like behavior at higher θ gives way to a sudden and dramatic increase in penetration depth when $\theta \lesssim 1$. A progressive increase in the penetration depth is measured as θ is further decreased, which corresponds to the distorted v' perturbations reported in Fig. 2.

We note that on the basis of the theoretical phase diagram proposed by Page and Zaki [16] for wavy plane-Couette flow, the weakly elastic fluid A is also expected to show transcritical behavior in the shallow channel since $\alpha \approx 1$ and $\Sigma = 0.1$ (i.e., $\alpha > \Sigma$ and $\Sigma < \pi$). However, experimentally we cannot capture a difference between polymer solution and Newtonian fluid in the shallow Poiseuille configuration. This is a consequence of the Newtonian v' perturbation spanning the entire flow domain for all θ in shallow channels [23]; hence, it is simply not possible to observe any increase in penetration when a viscoelastic fluid is employed. For the same reason, inviscid type behavior is also not apparent in shallow channels (either experimentally or in theory) when the penetration depth is assessed using the v' perturbation. Theory indicates that the full vorticity perturbation (which decays closer to the wall) is required to observe these phenomena in shallow channels [23].

The distinctive property of the transcritical regime is the spanwise vorticity generated at a finite distance $l_c < d$ from the wall. Since the spanwise vorticity field is not extracted from the experimental data, some supporting linear results for Poiseuille flow in the deep $\alpha = 3.2\pi$ channel are provided in Fig. 4. The reported perturbation velocities and spanwise vorticity were obtained from the linearized perturbation equations for an Oldroyd-B fluid. In the linear theory, the small-amplitude surface waviness of the experimental channel appears as a periodic slip condition on the streamwise velocity at first order in an asymptotic expansion in powers of the wave amplitude (e.g., see Refs. [16,17,23]). These linear results were computed at the experimental value of $\beta = 0.96$ with $\theta \ll 1$ and $\mathrm{Wi} \gg 1$ to emphasize the vorticity amplification effect. Note that, in this limit, the

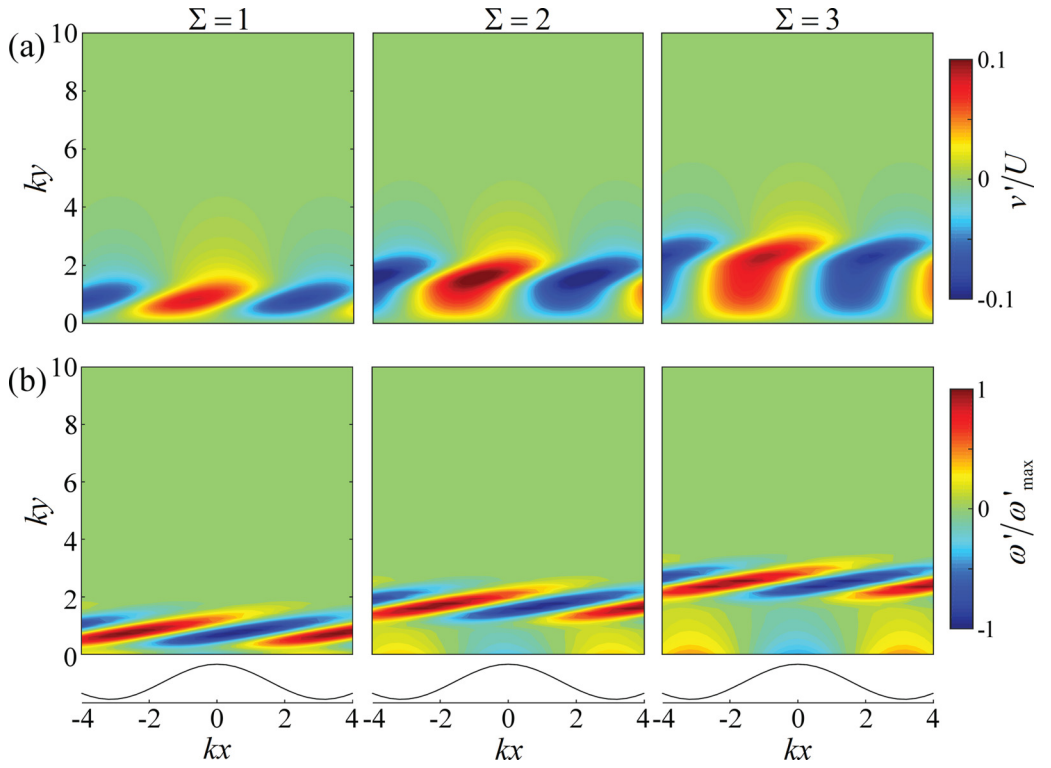

FIG. 4. (a) Normalized transverse velocity and (b) spanwise vorticity perturbations predicted by the linear equations in the elastic-Rayleigh limit (Wi $\gg 1$, $\theta \ll 1$) in a deep channel ($\alpha = 3.2\pi$). In all three cases $\beta = 0.96$. A finite Reynolds number regularizes the solution at the critical layer. The critical layer is centered about a dimensionless distance $ky = \Sigma$, in agreement with Ref. [16].

Newtonian perturbation $v'_{\text{Newt}} = O(\theta)$ and hence cannot be contrasted with the viscoelastic flows as was done in Fig. 2. In viscoelastic fluids, the limit $\theta \ll 1$, Wi $\gg 1$ leads to an elastic-Rayleigh equation [16,27,28] that depends on Σ alone. While fluid A has $\Sigma = 1$, three values were used in the Oldroyd-B model, $\Sigma = \{1, 2, 3\}$. The v'-perturbation fields shown in Fig. 4(a) share qualitative similarities with the experimental v' fields reported in Fig. 2(b). Furthermore, all three values of Σ show vorticity amplification in tilted stripes at the critical layer $ky = \Sigma$. This indicates that the non-Newtonian v' fields measured experimentally are consistent with the modification of v' fields expected due to the theoretically predicted vorticity amplification in the transcritical regime. Hence, the images shown in Figs. 2(b) and 2(c) represent a manifestation of the critical layer as observed in the experimental velocity field. We define a quantity $\mathcal{P}' = \mathcal{P}_{\text{pol}} - \mathcal{P}_{\text{Newt}}$ to compare the penetration of a polymer solution, $\mathcal{P}_{\text{pol}}$, and that of Newtonian fluid $\mathcal{P}_{\text{Newt}}$. The linear theory predicts that $\mathcal{P}' \to \Sigma$, as Wi $\to \infty$ with Σ held fixed. The inset of Fig. 3 shows $\mathcal{P}'$ for polymeric fluid A in the deep channel. Consistent with theory, $\mathcal{P}'$ tends toward a plateau as Wi increases, and experimentally $\mathcal{P}' \to 3\Sigma$.

The present work provides the first physical evidence that dilute polymeric flow at high Wi and Re over wavy surfaces can lead to the generation of critical layers away from the site of disturbance. Such critical layers were predicted only recently by linear theory, which shows they drive significant amplification of the spanwise vorticity. The experiments reported here demonstrate that these critical layers have measurable effects in real flows with real viscoelastic fluids. Despite the simplicity of the viscoelastic model and the assumptions invoked in the theory, predicted velocity fields show good qualitative agreement with the experiment. The experiment thus validates the theory,

indicating that the critical layer is a robust but hitherto overlooked feature of inertioelastic flows with streamline curvature. The consequences are potentially profound, and recognizing the existence of these vorticity amplification phenomena may shed important insight into the mechanisms of a wide range of inertioelastic flows, such as turbulent drag reduction and EIT.

S.J.H. and A.Q.S. gratefully acknowledge the support of the Okinawa Institute of Science and Technology Graduate University (OIST) with subsidy funding from the Cabinet Office, Government of Japan. S.J.H. and A.Q.S. also acknowledge funding from the Japan Society for the Promotion of Science (Grants-in-Aid for Scientific Research (C), Grants No. 18K03958 and No. 17K06173, respectively). Kazumi Toda-Peters from OIST is thanked for device fabrication. S.J.H. is grateful to TA Instruments for the donation of a DHR3 rheometer through their Distinguished Young Rheologist Award. T.A.Z. acknowledges support from the National Science Foundation (Grant No. 1511937).

[1] D. F. James and J. H. Saringer, Extensional fow of dilute polymer solutions, J. Fluid Mech. **97**, 655 (1980).
[2] J. J. J. Gillissen, Viscoelastic flow simulations through an array of cylinders, Phys. Rev. E **87**, 023003 (2013).
[3] P. S. Virk and H. Baher, The effect of polymer concentration on drag reduction, Chem. Eng. Sci. **25**, 1183 (1970).
[4] L. Xi and M. D. Graham, Dynamics on the Laminar-Turbulent Boundary and the Origin of the Maximum Drag Reduction Asymptote, Phys. Rev. Lett. **108**, 028301 (2012).
[5] S. J. Lee and T. A. Zaki, Simulations of natural transition in viscoelastic channel flow, J. Fluid Mech. **820**, 232 (2017).
[6] M.-N. Wei, B. Li, R. L. A. David, S. C. Jones, V. Sarohia, J. A. Schmitigal, and J. A. Kornfield, Megasupramolecules for safer, cleaner fuel by end association of long telechelic polymers, Science **350**, 72 (2015).
[7] B. Keshavarz, E. C. Houze, J. R. Moore, M. R. Koerner, and G. H. McKinley, Ligament Mediated Fragmentation of Viscoelastic Liquids, Phys. Rev. Lett. **117**, 154502 (2016).
[8] M. I. Smith and V. Bertola, Effect of Polymer Additives on the Wetting of Impacting Droplets, Phys. Rev. Lett. **104**, 154502 (2010).
[9] K. Kim, C.-F. Li, R. Sureshkumar, S. Balachandar, and R. J. Adrian, Effects of polymer stresses on eddy structures in drag-reduced turbulent channel flow, J. Fluid Mech. **584**, 281 (2007).
[10] K. Kim and R. Sureshkumar, Spatiotemporal evolution of hairpin eddies, Reynolds stress, and polymer torque in polymer drag-reduced turbulent channel flows, Phys. Rev. E **87**, 063002 (2013).
[11] N. Burshtein, K. Zografos, A. Q. Shen, R. J. Poole, and S. J. Haward, Inertioelastic Flow Instability at a Stagnation Point, Phys. Rev. X **7**, 041039 (2017).
[12] D. Samanta, Y. Dubief, M. Holzner, C. Scäfer, A. N. Morozov, C. Wagner, and B. Hof, Elasto-inertial turbulence, Proc. Natl. Acad. Sci. USA **110**, 10557 (2013).
[13] Y. Dubief, V. E. Terrapon, and J. Soria, On the mechanism of elasto-inertial turbulence, Phys. Fluids **25**, 110817 (2013).
[14] P. Pakdel and G. H. McKinley, Elastic Instability and Curved Streamlines, Phys. Rev. Lett. **77**, 2459 (1996).
[15] A. Groisman and V. Steinberg, Elastic turbulence in a polymer solution flow, Nature (London) **405**, 53 (2000).
[16] J. Page and T. A. Zaki, Viscoelastic shear flow over a wavy surface, J. Fluid Mech. **801**, 392 (2016).
[17] F. Charru and E. J. Hinch, "Phase diagram" of interfacial instabilities in a two-layer Couette flow and mechanism of the long-wave instability, J. Fluid Mech. **414**, 195 (2000).
[18] D. D. Joseph, M. Renardy, and J. C. Saut, Hyperbolicity and change of type in the flow of viscoelastic fluids, Arch. Rat. Mech. Anal. **87**, 213 (1985).

[19] J. Y. Yoo and D. D. Joseph, Hyperbolicity and change of type in the flow of viscoelastic fluids through channels, J. Non-Newtonian Fluid Mech. **19**, 15 (1985).
[20] M. Ahrens, J. Y. Yoo, and D. D. Joseph, Hyperbolicity and change of type in the flow of viscoelastic fluids through pipes, J. Non-Newtonian Fluid Mech. **24**, 67 (1987).
[21] H. H. Hu and D. D. Joseph, Numerical simulation of viscoelastic flow around a cylinder, J. Non-Newtonian Fluid Mech. **37**, 347 (1990).
[22] V. Delvaux and M. J. Crochet, Numerical prediction of anomalous transport properties in viscoelastic flow, J. Non-Newtonian Fluid Mech. **37**, 297 (1990).
[23] S. J. Haward, A. Q. Shen, J. Page, and T. A. Zaki, Poiseuille flow over a wavy surface, Phys. Rev. Fluids **2**, 124102 (2017).
[24] G. Meineke, M. Hermans, J. Klos, A. Lenenbach, and R. Noll, A microfluidic opto-caloric switch for sorting of particles by using 3D-hydrodynamic focusing based on SLE fabrication capabilities, Lab Chip **16**, 820 (2016).
[25] C. D. Meinhart, S. T. Wereley, and M. H. B. Gray, Volume illumination for two-dimensional particle image velocimetry, Meas. Sci. Technol. **11**, 809 (2000).
[26] S. T. Wereley and C. D. Meinhart, Recent advances in micro-particle image velocimetry, Annu. Rev. Fluid Mech. **42**, 557 (2010).
[27] J. Azaiez and G. M. Homsy, Linear stability of free shear flow of viscoelastic liquids, J. Fluid Mech. **268**, 37 (1994).
[28] P. K. Ray and T. A. Zaki, Absolute instability in viscoelastic mixing layers, Phys. Fluids **26**, 014103 (2014).